J. Fluid Mech. (1992), *vol.* 245, *pp.* 191–210

Measurements of the interaction of wave groups with shorter wind-generated waves

By JACOB S. CHU[1], STEVEN R. LONG[2] AND O. M. PHILLIPS[1]

[1] Department of Earth and Planetary Sciences, The Johns Hopkins University, Baltimore, MD 21218, USA

[2] NASA Goddard Space Flight Center, Wallops Flight Facility, Wallops Island, VA 23337, USA

(Received 27 September 1991)

Fields of statistically steady wind-generated waves produced in the NASA-Wallops wind wave facility, were perturbed by the injection of groups of longer waves with various slopes, mechanically generated at the upwind end of the tank. The time histories of the surface displacements were measured at four fetches in ensembles consisting of 100 realizations of each set of experimental conditions, the data being stored and analysed digitally. The overall interaction was found to have four distinct phases. (i) When the longer waves overtake the pre-existing wind-generated waves, during the first half of the group where successive crests are increasing in amplitude, vigorous wave breaking near the crests reduces the energy density and $\overline{\zeta^2}$ in the wind waves while straining by the orbital velocities of the group reduces their wavelengths near the crests; the 'significant slope' $2\pi(\overline{\zeta^2})^{\frac{1}{2}}/\lambda$ at the crests is found to be very nearly constant and equal to the initial, undisturbed value. After the maximum wave of the group has passed, breaking appears to virtually cease but the earlier energy loss results in suppression of the short waves. The overall suppression by a group of waves is significantly less than that measured by Mitsuyasu (1966) and Phillips & Banner (1974) in a continuous train of waves whose slope is equal to the maximum in the group. A simple description of this phase of the interaction, involving constant significant slope of the breaking waves over the leading half of the group and conservation of action thereafter, gives suppression ratios close to those measured. (ii) Once the group has passed, the surface is much smoother and the waves begin to regenerate under the continued influence of the wind but at rates considerably slower than those suggested by Plant's formula, using the averaged value of u_*. This is qualitatively consistent with a locally reduced surface stress as the wind blows from rougher water well behind the group to the smoother surface immediately behind it. (iii) The regeneration is interrupted by the arrival of a wave energy front moving down the tank, across which the energy density rises abruptly to values up to six times greater than in the undisturbed field. At the same time, the dominant frequencies just behind the wave energy front are lower than in the initial field, and the significant slope $(\overline{\zeta^2})^{\frac{1}{2}}\,\sigma^2/g$ is, within experimental uncertainty, again identical to that in the initial field. The front was found to propagate notably faster than the appropriate group velocity $(g/2\sigma)$ and it is suggested that this is the combined result of dispersion, nonlinearity and wind amplification, together with wind-induced drift in the tank. Finally, (iv) the energy density gradually subsides and the dominant wave frequency increases as the wind waves relax towards their undisturbed state, the relaxation seeming to be essentially complete when energy packets arriving at a point have originated at the upwind end of the tank, rather than at the wave energy front.

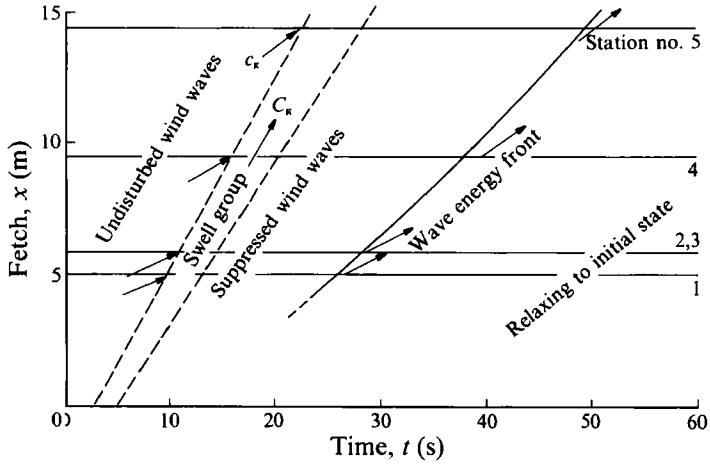

FIGURE 1. An x–t diagram describing the experiment. The locations of the measurement stations are represented by the horizontal lines and the arrows indicate the speeds of energy propagation.

1. Introduction

It has long been known that when a continuous train of mechanically generated long waves is superimposed on shorter, wind-generated waves, there can be a substantial reduction in the average spectral density of the shorter waves from the levels that are found under the same conditions but in the absence of the swell. The phenomenon seems to have been observed first by Mitsuyasu (1966) and was further studied by Phillips & Banner (1974) and Donelan (1987), but there is no consensus about the mechanisms involved. Phillips & Banner attributed the reduction in the case of short gravity waves to enhanced microscale breaking with dissipative, parasitic capillaries when the wind-drift velocity at the surface is amplified near the long-wave crests. Donelan on the other hand suggested that detuning of the resonance conditions for weak nonlinear interactions among the wind waves, brought about by the long-wave straining, may be the dominant cause. He noted that the direct wind input to the shorter waves appeared to be insensitive to the presence of the longer ones.

All of these experiments involved a continuous train of mechanically generated waves, in whose presence the shorter wind-generated wave field developed. It occurred to us that the nature of the mechanism might be clarified if the wind waves were subjected to the passage of a group of longer waves rather than a continuous train of them. Enhanced wave breaking provides a rapid energy loss and if this is the process responsible, the reduction in energy density should also be found after a long-wave group had passed. On the other hand, wave–wave interactions have timescales vey much longer than the wave period, so that the disruption of them as the group passes should have little net effect.

The experiments described here, then, involve a pre-existing, statistically steady wind-wave field in a laboratory wind-wave facility into which, at the upstream end, groups of longer, mechanically generated waves are injected, the time histories of the wave fields being measured at various points down the tank before, during and after the passage of the groups. Because of the randomness of the wind-generated waves

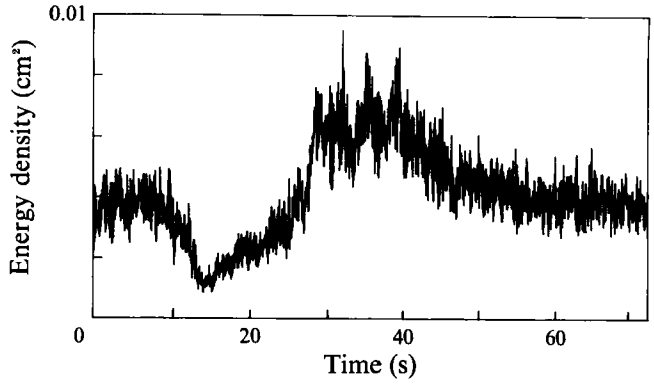

FIGURE 2. A characteristic record of the mean-square surface displacement of the shorter windwaves at a fixed point, averaged over an ensemble of 100 realizations. The long-wave group, which has been filtered out, passes this point in the interval between 8 and 14 s.

and the absence of stationarity, it was necessary to repeat each experiment a large number of times (100), recording the data digitally in order to obtain ensemble averages. Although initially motivated by the questions described above, the experiment revealed a number of different phenomena and several surprises, and to put them into context, it is probably clearest to give an overview here of what we have found, before embarking on a detailed description of the various phases of the interaction.

The x–t diagram of figure 1 provides a 'road map', with fetch down the tank plotted vertically and elapsed time horizontally. Initially, there is a statistically steady field of wind waves growing with fetch; the stationary observation points are indicated by the horizontal lines. A group of longer waves is then generated at zero fetch and passes down the tank, moving with its group velocity, catching up and overtaking the wind waves whose group velocity is less. Figure 2 represents the time history at a fixed point of the mean-square surface displacement of the short waves in a typical experiment, averaged over the ensemble of 100 realizations. Clearly, the wind waves are suppressed immediately, during the passage of the group, beyond which they begin to recover under the continued action of the wind. However, to our surprise we found that after some time the energy density rises abruptly to levels considerably higher than those which existed in the initial, undisturbed field, after which it gradually relaxes back towards the initial state.

This overshoot we attribute not to local generation but to the passage of a wind-wave energy front, which seems to be a new phenomenon. Spectra, calculated from short segments of the records and also averaged over the 100 realizations are shown in figure 3; the dominant frequency of the wind wave is unaltered by the suppression but immediately behind the wave energy front it is significantly less than in the initial field – the waves here are longer as well as higher. We found that the front propagates somewhat faster than one would expect even at this lower frequency, a fact that we will attribute to the combined effect of dispersion, wind input and wind-induced drift. In the final state, the spectrum returns to its initial form. Although its details varied, this overshoot was found under all of the conditions that we investigated; it seems to be a robust phenomenon, at least in this wind-wave facility. A hint of its existence is indeed to be found in unpublished fragmentary results obtained by Ms Kaye Burnett in a similar experiment some ten years ago involving only three realizations (this was before the time of high-powered data processing).

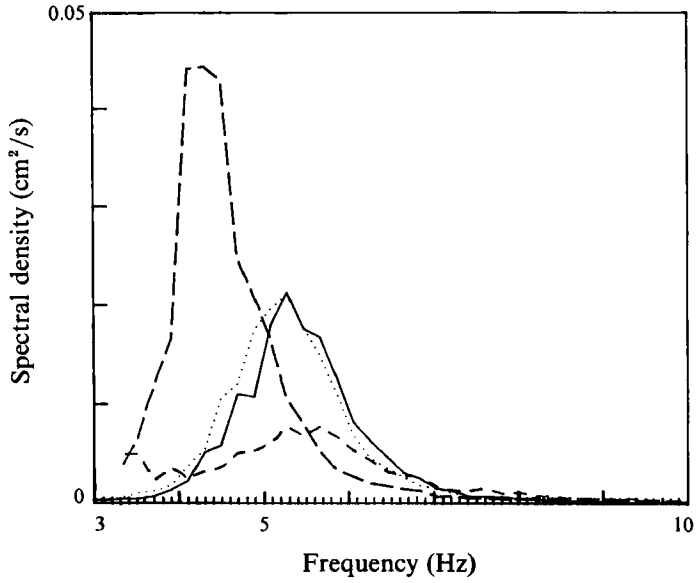

FIGURE 3. Short-period spectra, measured at a fetch of 5.9 m with $u_* = 27$ cm s^{-1}, of the wind-generated waves before the arrival of the group (———); immediately following the group (– – – –); immediately behind the wave energy front (——), and about 60 s after the wave energy front (.....), the spectrum then having returned to its initial form.

She noted that the short-wave energy density seemed to rise abruptly some time after the passage of a group, though with only three realizations the statistical significance was low.

In the following sections we describe the conditions of the experiment in more detail, methods of data acquisition, extraction of ensemble averages and the characteristics of the initial wave field. In the phase of interaction between the short waves and the long-wave group, we separate the random wind waves from the (almost) deterministic and much more energetic group to examine the kinematical and dynamical response of the wind waves inside the group. Following the encounter, the recovery phase enables us to estimate energy input rates from the wind. Finally, the properties of the wave energy front are documented and a preliminary discussion is given of the dynamical processes involved in its formation.

2. Description of the experiment

2.1. *Procedure*

The experiments were conducted in the NASA-Wallops wind-wave facility described by Huang & Long (1980). The test section is 18.29 m long, 1.22 m high and 0.76 m wide, filled with water to a depth of 0.76 m with 0.45 m remaining for the air flow above. The air flow was drawn across the water surface by a fan beyond the downwind end of the tank and returned in a closed circuit. At a distance 0.27 m from the upwind end of the tank a wavemaker was emplaced across the tank, which was a rigid plate with a total height of 30.5 cm, 5 cm of which projected above the water surface and provided something of a trip to the air flow. At the bottom of the rigid plate was a flexible plastic skirt extending a further 16 cm down. The wavemaker oscillated rectilinearly, driven by a hydraulic system using electro-servo-valves with an error-

u_* (cm s^{-1})	f (Hz)	$(ak)_m$
0	1.25	0.10, 0.16, 0.23
15	1.25	0.10–0.11, 0.15–0.18, 0.23–0.35
15	1.5	0.25
27	1.25	0.12–0.16, 0.23–0.25, 0.26–0.38

TABLE 1. Conditions investigated: f = frequency of the wave group, $(ak)_m$ = maximum slope. Fetches: 5.2, 5.9, 9.5 and 14.4 m.

correcting feedback loop. The system was capable of following any input signal within the range ± 10 V over frequencies less than 10 Hz, though the rather unconventional design gave clean wave pulses only in a fairly narrow frequency range between 1.25 and 2 Hz. At the downwind end, a sloping plastic honeycomb served as a beach to absorb incident wave energy, the reflectivity over the amplitudes and wavelengths used being approximately 3%.

Mean velocities in the air stream were measured at fetches of 6.75 m and 9.8 m using Datametrics differential pressure transducers attached to Pitot tubes that were used to measure the wind speed at heights between 8 and 18 cm above the still water level, the friction velocities being extracted by Gauss–Newton fits to a logarithmic profile. Two wind speed settings were used in these experiments, with average values of u_* at the two stations of 15 and 27 cm s^{-1}.

Measurements of the surface displacement ζ were made using a set of capacitance wire gauges at various fetches. These had a nominal sensitivity of ± 0.035 mm and a good linear response (see Huang & Long 1980). Data from the probes were digitized every 10 ms and the gauges were intercalibrated by making simultaneous measurements in a mechanically generated 2 Hz wave train, applying a separate calibration factor to the data stream from each to equalize the values of $\overline{\zeta^2}$.

The long-wave groups were generated by modulating a series of seven sinusoidal waves by a sech^2 envelope with a chosen peak amplitude, the profile being stored digitally with a resolution of 1°. These data were sent to a digitial-to-analog converter which supplied the wave-packet voltage history to the wavemaker electronics, which in turn controlled the production of the wave packet by the hydraulic unit. The computer kept track of the time, commencing the data acquisition 3 s before the paddle motion began and continuing for 72 s in early series, 120 s in the later series but in a few experiments longer (160 s), archiving the digitized data to hard disk as a numbered realization, waiting a specified time, usually 188 s to allow the tank to return to its undisturbed state of purely wind-generated waves and then repeating the cycle until the ensemble of 100 realizations had accumulated. The choice of 100 realizations was a compromise between the desire for reasonable accuracy (about $n^{-\frac{1}{2}}$ or 10% in $\overline{\zeta^2}$) and reasonable duration for each set of experimental conditions (overnight). The range of conditions studied is listed in table 1.

2.2. *Ensemble averaging within the long-wave group*

One objective of these experiments was to examine the characteristics of the wind-generated waves during the passage of a mechanically generated wave group. If the latter were precisely identical in each realization, its profile at each measurement station would be defined exactly by the average $\bar{\zeta}(t)$, over the realizations, and the

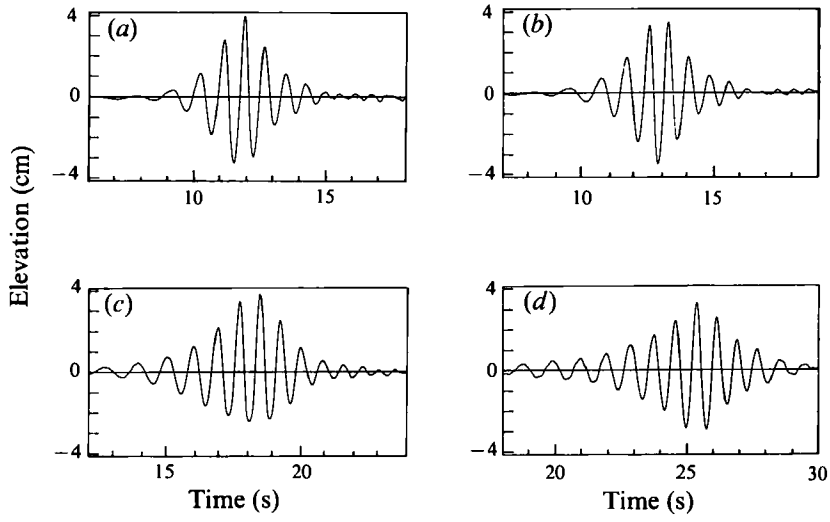

FIGURE 4. Ensemble averages of the wave groups at fetches (*a*) 5.2, (*b*) 5.9 (*c*), 9.5 and (*d*) 14.4 m with $u_* = 15$ cm s^{-1}.

random, wind-generated component in each realization as the difference $\zeta' = \zeta - \bar{\zeta}$. However, the maximum amplitude of the group ranged among the experiments between 1.5 and 3 cm while the r.m.s. wind wave height was only about one-tenth of this, so that small differences in the wave group profile among realizations can produce substantial errors in the estimate of ζ'. The groups were indeed generated to be as precisely identical as the mechanical and electronic systems allow and the time was accurate to within 20 ms. Individual groups were separated in time by about 5 min, so that there was no contamination by reflected waves, but wave breaking certainly generated small-scale turbulence in the water and possibly low-frequency currents that could modify the propagation characteristics of the group somewhat, introducing phase and possibly amplitude variations or jitter among the realizations in an ensemble, that accumulate with fetch. Thus if at any measurement station

$$\zeta(t) = \alpha(t)(1+\Delta)\cos(nt+\epsilon)+\zeta'(t), \tag{2.1}$$

where $\alpha(t)$ is the profile in time of the group envelope, Δ and ϵ are small errors in amplitude and phase and ζ' is the wind-wave component, then

$$\bar{\zeta} = \alpha(t)(\cos nt + O(\epsilon^2)) \tag{2.2}$$

and

$$\overline{(\zeta-\bar{\zeta})^2} = \overline{\zeta'^2}+\alpha^2(t)\{\overline{\Delta^2}\cos^2 nt+\overline{\epsilon^2}\sin^2 nt+2\overline{\epsilon\Delta}\sin nt\cos nt\} \tag{2.3}$$

to the lowest order in $\overline{\epsilon^2}$, $\overline{\Delta^2}$.

Examples of the ensemble averages $\bar{\zeta}$ at the four fetches with $u_* = 15$ cm s^{-1} are shown in figure 4. The wave group disperses somewhat and the peak amplitude decreases by about 10% but it clearly maintains its identity as it propagates down the tank. The time intervals between successive crests of troughs in the leading portion of the group is up to 20% greater than in the central part, as is consistent with linear dispersion. The energy propagation speeds, estimated from the time intervals required for a given frequency to propagate from one measurement station to the next were consistently greater than the appropriate group velocity by 2–3 cm s^{-1} (3–5%) even when corrected for amplitude dispersion (see Whitham 1974), suggesting the presence of some wind-induced circulation in the tank. Figure 5 shows

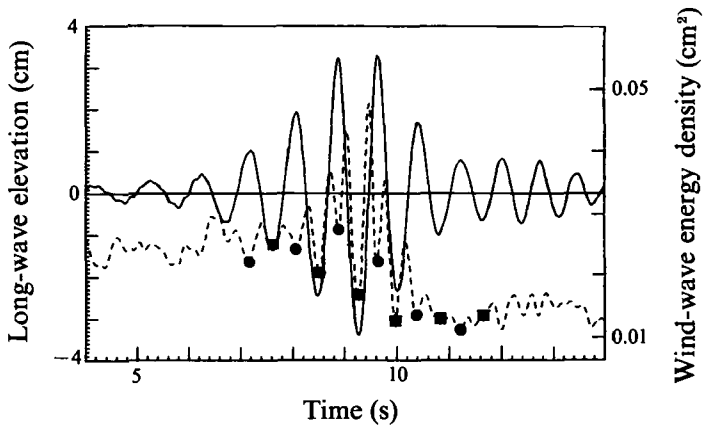

FIGURE 5. Modulation and oscillation of $\overline{\zeta'^2}$ for the short waves (----) during the passage of the long-wave groups, whose mean profile is shown by the solid line. Values of $\overline{\zeta'^2}$ at the crests of the group are marked by squares, at the troughs by circles.

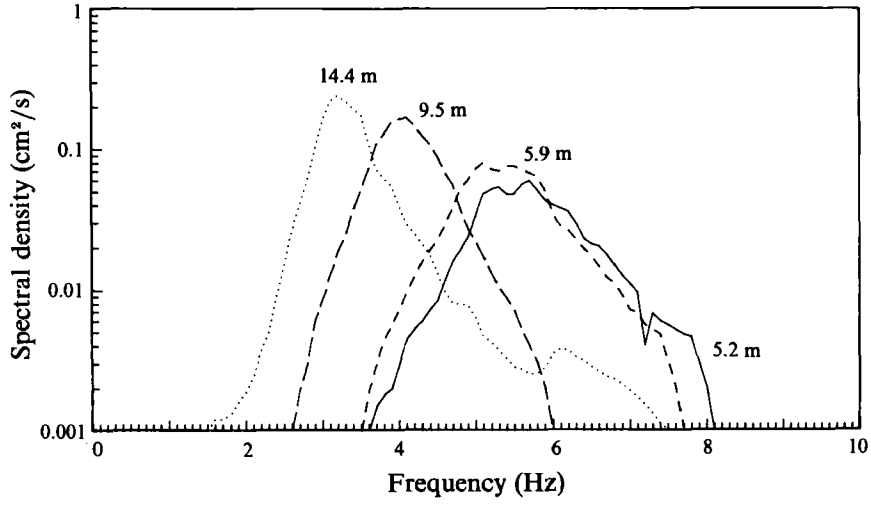

FIGURE 6. Spectra of undisturbed wind waves in the tank at the four fetches, $u_* = 27$ cm s^{-1}.

the variations in the ensemble average $\overline{(\zeta-\bar{\zeta})^2}$ together with $\bar{\zeta}$ in a typical experiment, the fetch in this case being 5.9 m, the friction velocity 15 cm s^{-1} and the maximum group amplitude 3.3 cm. It is quite apparent that $\overline{(\zeta-\bar{\zeta})^2}$ oscillates at twice the frequency of the group, having maxima at the zero crossings of $\bar{\zeta}$ where $\cos nt = 0$, and minima at the crests and troughs, where $\sin nt = 0$. This indicates that $\overline{\epsilon^2} \gg \overline{\Delta^2}$, the phase jitter being the dominant error. From the amplitude of the oscillation in $\overline{(\zeta-\bar{\zeta})^2}$, $(\overline{\epsilon^2})^{\frac{1}{2}}$ can be found from (2.3) to be about 0.05 or 2.5°, developed over some 18 cycles of propagation. Variations of this magnitude seem not at all surprising and they would be expected to increase with fetch. Fortunately, however, the smallness of $\overline{\Delta^2}$, inferred from the phase of the oscillations relative to $\bar{\zeta}$, implies that the values of $\overline{(\zeta-\bar{\zeta})^2}$ at the minima where $\sin^2 nt = 0$ (i.e. at the crests and troughs of the waves of the group) were only slightly larger than the true value of $\overline{\zeta'^2}$ for the wind-generated waves. Only these values were used in the subsequent analysis. They enabled us to trace the differences in $\overline{\zeta'^2}$ at the crests and troughs in

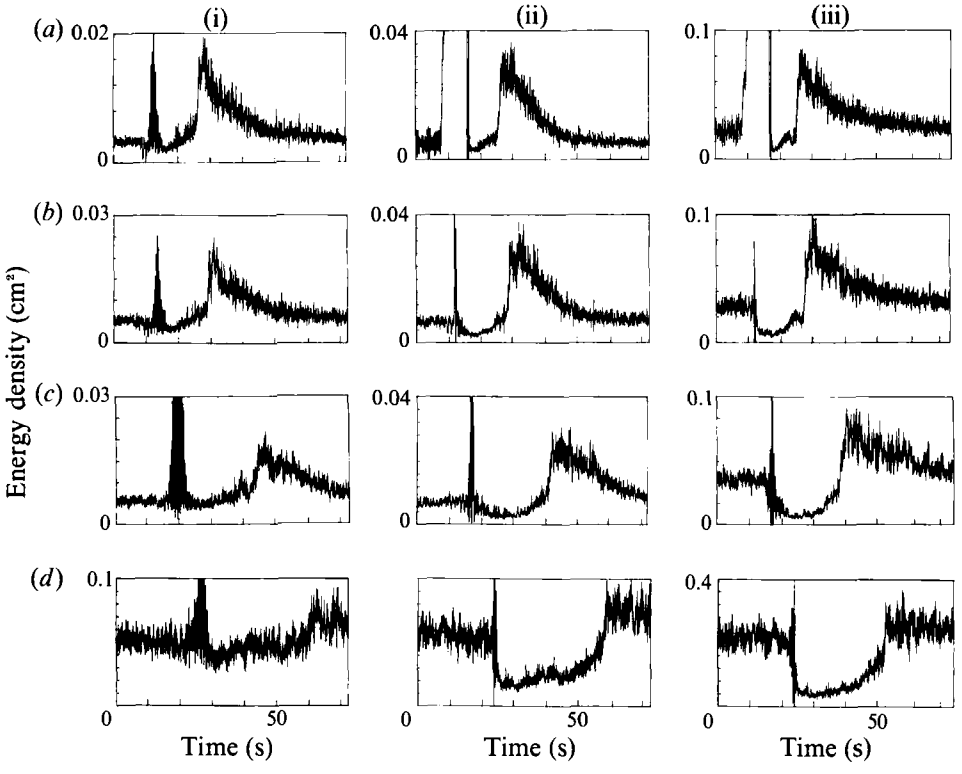

FIGURE 7. Time histories of $\overline{\zeta'^2} = \overline{(\zeta-\bar{\zeta})^2}$ at fetches of (*a*) 5.2 m, (*b*) 5.9 m, (*c*) 9.5 m and (*d*) 14.4 m. Column (i) is for $u_* = 15$ cm s^{-1} and maximum slope of the groups $(\alpha k)_m = 0.10$; column (ii), $u_* = 15$ cm s^{-1} and $(\alpha k)_m = 0.26$; (iii) $u_* = 27$ cm s^{-1}, $(\alpha k)_m = 0.26$.

a good number of the experiments, but in some of them, particularly at the larger fetches and higher wind speeds, the oscillations in $\overline{(\zeta-\bar{\zeta})^2}$ during the interaction were so extreme that they were not useful in this regard.

Similarly, in the extraction of variations of $\overline{(\delta\zeta'/\delta t)^2}$ during the passage of the group, when $\overline{A^2} \ll \overline{\epsilon^2}$

$$\overline{\left[\frac{\delta}{\delta t}(\zeta-\bar{\zeta})\right]^2} = \overline{\left(\frac{\delta\zeta'}{\delta t}\right)^2} + \overline{\epsilon^2} n^2\alpha^2 \cos^2 nt, \tag{2.4}$$

with terms involving $\dot{\alpha} \ll na$ being neglected. In this case, the frequency ratio between the wind-generated waves and those in the group (characteristically about 4) reduces the relative error by the square of this ratio. In experiments from which $\overline{\zeta'^2}$ during the interaction could be measured, oscillations in the measured quantity on the left-hand side of (2.4) at frequency $2n$ were imperceptible, being within the general 10% random error level.

3. The overall response of the wind-wave field

The undisturbed wind-wave field was similar to those generated at short fetches in other facilities of this kind. The spectra of figure 6 evolve characteristically with fetch, showing overshoot at high frequencies as the dominant frequency decreases.

Samples of the time histories of $\overline{(\zeta-\bar{\zeta})^2}$ measured at the four fetches are exhibited in figure 7. The main features of the patterns are strikingly consistent. In these particular experiments, the passage of the wave group is marked by the large

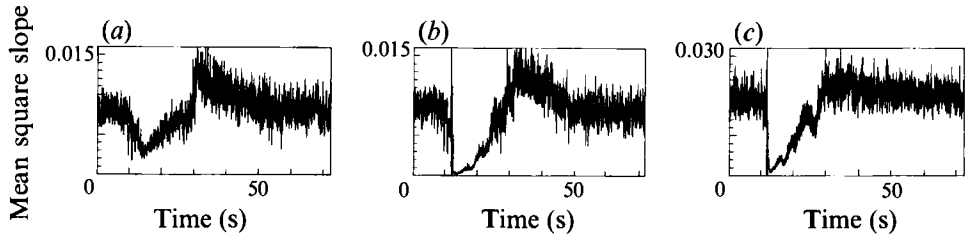

FIGURE 8. Time histories of mean-square slope measured by two probes separated by 1 cm, in the experiments of figure 7(*b*). The fetch was 5.9 m; in (*a*, *b*) $u_* = 15$ cm s^{-1} and in (*c*) $u_* = 27$ cm s^{-1}. The maximum slope of the long-wave group was 0.10 in the (*a*) and 0.26 in (*b*, *c*).

oscillations or data dropouts caused by phase jitter in $\bar{\zeta}$; these do serve to mark the location of the wave group as it passes down the tank. A comparison between figures 7(i) and 7(ii) shows that the relative suppression of the wind wave increases with the slope of the group, as found by Mitsuyasu (1966) and by Phillips & Banner (1974) for a continuous train of long waves. The energy loss clearly occurs within the group and this will be examined in more detail in the next section. Following a period in which the waves regenerate to a greater or lesser extent, the wave energy front arrives, moving more slowly than the group since the time interval between the group and the front increases with fetch. The energy density in the front relative to that in the undisturbed field decreases with increasing fetch, or equivalently, with increasing energy density in the regenerated waves immediately preceding it. When $u_* = 15$ cm s^{-1} at the shortest fetch the energy level in the front following a group with $(ak)_m = 0.10$ is four or five times greater than in the undisturbed field. At a fetch of 14.4 m, both energy densities are greater but the ratio is now only about 1.5. A comparison between the figures 7(ii) and 7(iii) suggests that the ratio is greater at low wind speeds, when the initial wave field is of course less energetic. The arrival time of the front is noticeably earlier when $u_* = 27$ cm s^{-1} than it is when $u_* = 15$ cm s^{-1}, so that its propagation speed increases with wind stress.

At the fetch of 5.9 m, two wave probes separated by 1 cm in the wind direction allowed measurements of the instantaneous surface slope on scales larger than this, by the difference in the two signals. The nominal sensitivity of this slope measurement was ± 0.05. Time histories of $\overline{(\delta\zeta'/\delta x)^2}$ estimated in this way are given in figure 8 for the three experiments of figure 7(*b*). The suppression of this measure of the slope is clearly much greater than that of $\overline{\zeta'^2}$ and this is consistent with the much smoother appearance of the water surface that could be seen behind the group. On the other hand, the mean-square slope in the wave energy front is only fractionally larger than in the undisturbed wave field even though $\overline{\zeta'^2}$ is several times larger, which implies that the local spectrum in the front is much narrower, lacking to a considerable extent the smaller-scale components in the initial spectrum.

This inference is confirmed by examination of local spectra, calculated from blocks of 256 points (about 5 s of record) in intervals in which the wave field was not changing too rapidly and averaged over the 100 realizations. Figure 3 is typical of these, and although the frequency discrimination is not good in the absence of strict stationarity and with such short record lengths, it is apparent that the dominant frequency in the interval just behind the energy front is lower than in the initial wave field (and in the suppressed waves). The spectrum is sharper, the ratio $\Delta\sigma/\sigma_0$ of spectral width at the half-energy level to peak frequency being 0.21 compared with an initial value of 0.25.

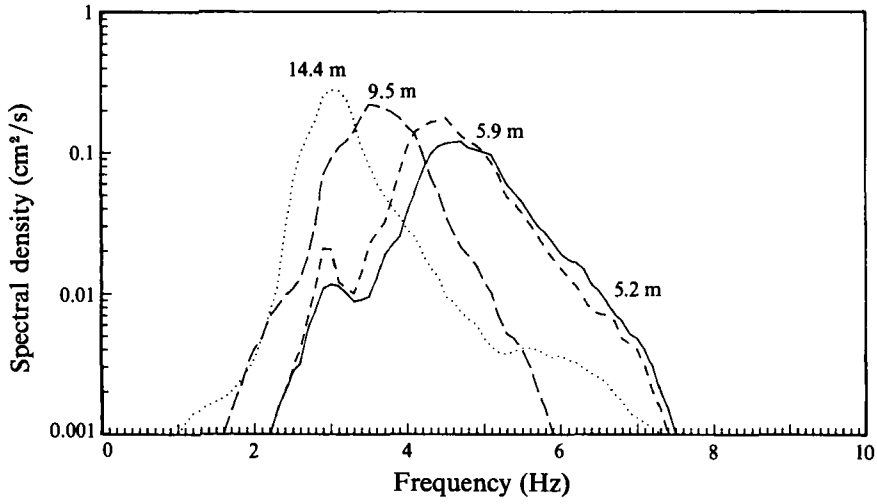

FIGURE 9. Local spectra measured immediately behind the wave energy front at the four fetches; $u_* = 27$ cm s^{-1}, $(\alpha k)_m = 0.16$.

In contrast, the slope of the dominant waves, defined as $(\overline{\zeta'^2})^{\frac{1}{2}}\sigma_0^2/g$ differs much less between the initial waves and the longer, higher waves in the front. The variations will be described in detail in §6 it suffices now to note that in the particular experiment of figure 3, this quantity was 0.28 initially and 0.24 in the front.

Behind the energy front, the waves at any measurement station gradually return to their initial state, with $\overline{\zeta'^2}$ decreasing and the dominant frequency increasing. The dominant frequency of the waves just behind the front decreases with increasing fetch (figure 9) and their group velocity increases; the front itself will be found to advance a little faster than this. Accordingly, at a fixed measurement station, at points in time successively behind the front, the dominant frequency increases, the corresponding group velocity decreases and the waves were generated along energy paths which originate at the energy front at successively greater distances upwind. Relaxation seems to be essentially complete when the origin of the energy paths reaches the upwind end of the tank, as in the undisturbed state.

4. The interaction phase

4.1. *Modulations in apparent frequency*

When shorter waves ride on longer waves or swell, their apparent frequency measured at a fixed point is modulated by advection by the orbital velocity of the latter. The apparent frequency distribution is determined essentially by the kinematics of the interaction (see, for example, Phillips 1981). In long waves of frequency n and slope αk, travelling in the same direction, the apparent frequency of short waves with intrinsic frequency σ at a crest is

$$\sigma_c/\sigma = 1+(\sigma/n)\,\alpha k(1+\alpha k),$$

and at a trough

$$\sigma_t/\sigma = 1-(\sigma/n)\,\alpha k(1-\alpha k),$$

so that

$$((\sigma_{c,t}/\sigma)-1)\,n/\sigma = \alpha k(1+\alpha k), \tag{4.1}$$

αk being taken as positive at a crest and negative at a trough.

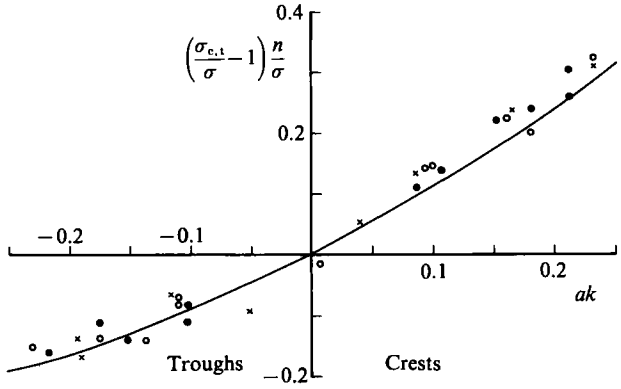

FIGURE 10. Wind-wave apparent frequencies σ measured at the crests and the troughs of the long-wave groups, of frequency n. ○, $n/\sigma = 0.25$, $u_* = 27$ cm s^{-1}; ● $n/\sigma = 0.22$, $u_* = 15$ cm s^{-1}; ×, $n/\sigma = 0.27$, $u_* = 15$ cm s^{-1}.

Because of the variation in apparent frequency with respect to phase of the long wave, the simplest way of determining a characteristic local frequency $\sigma_{c,t}/\sigma$ is to calculate the ratio of the ensemble-averaged quantities

$$[\overline{(\delta\zeta'/\delta t)^2}/\overline{\zeta'^2}]^{\frac{1}{2}} \tag{4.2}$$

at the crests and troughs, to the same quantity in the undisturbed wind-wave field before the arrival of the group. Measured values of these ratios were further averaged over $\pm 30°$ of a crest or trough to reduce the scatter somewhat, and the quantity on the left-hand side of (4.1) is shown as a function of ak in figure 10. At the crests the apparent frequencies are marginally higher than predicted by (4.1), probably as a result of the augmented wind drift there (Phillips & Banner 1974) but the general trend agrees well. Although this is not a very demanding test of the theory, it is perhaps of interest that this measure of the frequency follows the kinematics of the interaction in accordance with one's expectation, even though the short waves are breaking.

4.2. *Modulations in* $\overline{\zeta'^2}$.

In the absence of wave breaking, short waves are modulated by swell, with maximum values of $\overline{\zeta'^2}$ and local wavenumber at the crests and minima at the troughs. In the experiment (as in the field) the short waves are already breaking sporadically under the influence of the wind, and when they are overtaken by longer waves of successively increasing amplitude on the leading side of the group, they would be expected to break preferentially at each crest as the long-wave straining successively increases, while relaxing in the intervening troughs. Figure 11 shows values of $\overline{\zeta'^2}$ measured at the crests of the waves in the leading half of the group, referred to the initial undisturbed value, as a function of swell slope found from the amplitude of the associated crest. In these measurements, taken at the higher wind speed (u_*/c between 1.0 and 0.55, decreasing with fetch) the wind waves are not amplified by successively higher crests, but reduced, the rapid energy loss being evidently the result of enhanced breaking. The values of $\overline{\zeta'^2}$ in the troughs of the group were generally less than those in the crests, though the scatter of points in this part of the interaction did not allow a clear separation. Because of the straining of the short waves, their dominant wavelengths in the vicinity of the crests are also smaller. The slope of the dominant wind waves can be described by the 'significant slope',

$$2\pi(\overline{\zeta'^2})^{\frac{1}{2}}/\lambda = \sigma^2(\overline{\zeta'^2})^{\frac{1}{2}}/g' \tag{4.3}$$

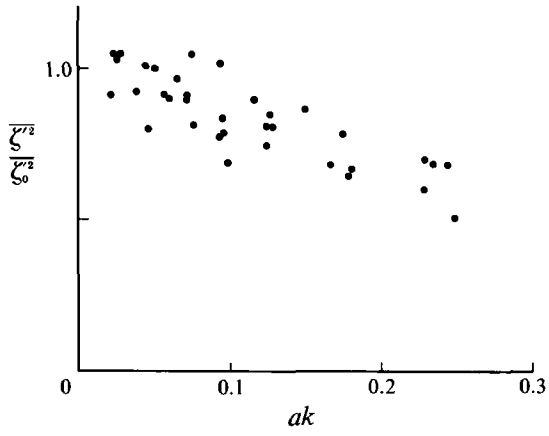

FIGURE 11. Mean-square displacements in the wind waves, normalized by the initial values, measured at the crests of the long waves in the leading portion of the group (with successively higher crests).

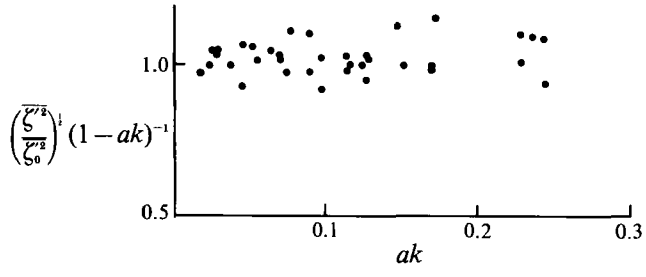

FIGURE 12. 'Significant slopes' of the wind waves relative to their initial values, measured at the crests of the long waves in the leading half of the group.

where $g' = g(1-\alpha k)$ is the effective gravitational acceleration that they experience at the crest of the long wave and σ is their intrinsic frequency which is very nearly constant with respect to phase of the long wave. The variation in significant slope at the successively growing long-wave crests in the first half of the group relative to the initial value is then given by $[(\overline{\zeta'^2})/(\overline{\zeta_0'^2})]^{\frac{1}{2}}(1-\alpha k)^{-1}$ and this quantity is shown in figure 12. The significant slope of the vigorously breaking waves appears to be very nearly constant; as they are shortened by the straining, their amplitude decreases in proportion, implying a high degree of geometrical similarity in the profiles of these breaking waves in the leading half of the overtaking wave group.

Once the highest waves of the group have passed, succesive crests are lower and troughs shallower. The wind waves have already been breaking at the crests on the leading side of the group, losing energy, so that on the trailing side of the group they are less energetic and less able to break at the successively decreasing crests. If all breaking ceased at the maximum of the group envelope, the wind waves thereafter should, in the frame of reference moving with the group crests, have approximately constant action flux, the wind input over the time interval involved being small. It can be shown simply that this would lead to a ratio of $\overline{\zeta'^2}$ in the second half of the group to that immediately following the group, $\overline{\zeta_1'^2}$, given by

$$\overline{\zeta'^2}/\overline{\zeta_1'^2} = (1-\alpha k\cos\chi)^{-2}, \tag{4.4}$$

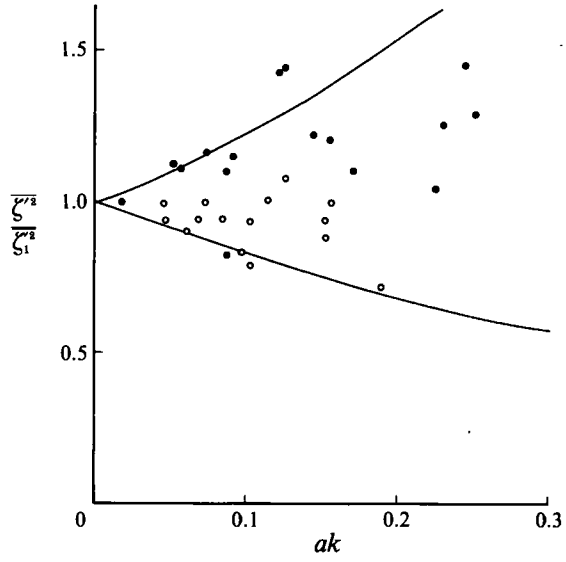

FIGURE 13. $\overline{\zeta'^2}$ for the wind waves relative to the values *following* the groups at the long-wave crests (solid symbols) and troughs (open symbols) in the rear half of the long-wave group.

where χ is the phase of the group wave. Figure 13 shows values of this ratio measured in five of the experimental runs, the crests ($\chi = 0$) being indicated by the solid symbols and the troughs by the open ones. The curves specify the ratios that would be expected if the action flux were indeed conserved and the wave motion entirely two-dimensional. Part of the scatter in measured values is probably the result of more sporadic residual surface disturbances following the earlier breaking (oblique wavelets, etc.). Nevertheless, the modulation between crests and troughs is evident from the separation of the solid and open symbols though it is less than predicted for purely two-dimensional waves.

In summary, the interaction between the longer-wave group and the wind-generated waves is characterized by vigorous wave breaking and rapid energy loss from the short waves over the first part of the group when the successive waves of the group are increasing in height. Breaking appears to virtually cease in the second part of the group where the waves are diminishing, the waves remaining after the group has passed having the same frequency as before (see in detail, figure 15 below) but being suppressed in their energy density.

4.3. *The overall suppression ratio*

It is evident from figure 7 that the relative suppresion of the wind waves increased with slope of the wave group with which they have interacted. Figure 14 shows measurements of the ratio of $\overline{\zeta^2}$ immediately after the passage of the group to that before, using the complete set of experiments, as a function of the maximum slope of the group. In order to eliminate any residual contribution to $\overline{\zeta^2}$ from the group itself, these values were found by integration of the short interval (256-point), ensemble-averaged spectra, over frequencies greater than that of the spectral minimum between the wind waves and the group (in the range 2.5 to 3.5 Hz among different experiments). Also plotted are the suppression ratios measured by Mitsuyasu (1966) and Phillips & Banner (1974) in continuous trains of mechanically generated waves.

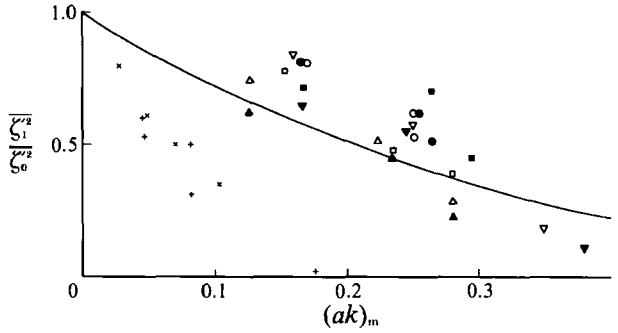

FIGURE 14. Overall suppression ratio of the wind waves as a function of maximum slope of the long-wave group. Fetches: △, 5.2 m; ▽, 5.9 m; ○, 9.5 m; □, 14.4 m; open symbols are for $u_* = 15$ cm s^{-1}, solid symbols for $u_* = 27$ cm s^{-1}. Also included are results from experiments with continuous trains of long waves: +, Phillips & Banner (1974); ×, Mitsuyasu (1968).

From this figure, it is clear that the suppression produced by a group of longer waves is less than that in a continuous wave train whose slope is equal to the maximum slope in the group. Presumably, this reflects the fact that in the latter case the short-wave energy packets are repeatedly subjected to the maximum straining at the long-wave crests with the more energetic wave groups repeatedly breaking, while in the former they experience this only once or twice. There appears to be no systematic dependence on u_* but possibly some dependence on fetch, the suppression often being somewhat greater at the larger fetches for a given $(\alpha k)_m$. The dominant frequency of the wind-generated waves decreases with fetch while that of the group does not, so that if this dependence is real, it presumably indicates a dependence on the frequency ratio of the interacting waves.

The conclusions of §§4.1 and 4.2 can be combined to provide an estimate of the overall suppression ratio. Since, from figure 12, the 'significant slope', equation (4.3), of the wind waves remains constant during their dissipation interval, at the point where the group envelope is a maximum,

$$\overline{\zeta^2} = \overline{\zeta_0^2}(1-(\alpha k)_m)^2,$$

and the energy density

$$\rho g'\overline{\zeta^2} = \rho g(1-(\alpha k)_m)\,\overline{\zeta^2} = \rho g(1-(\alpha k)_m)^3\,\overline{\zeta_0^2}.$$

If the energy dissipation from breaking of the short waves were to cease entirely after this point,

$$\overline{\zeta_1^2}/\overline{\zeta_0^2} = 1(-(\alpha k)_m)^3, \tag{4.5}$$

and this is indicated by the curve drawn in figure 14. This simple expression clearly overestimates the degre of suppression somewhat but it does conform to the general trend of the experimental results, adding some support to our conception of the sequence of events involved.

5. The recovery phase

Immediately after the long-wave group had passed, it was evident from visual observation and confirmed in the measurements of mean-square slope described in §3 that the water surface was notably smoother than it had been initially and very much smoother than it was during the interaction. The dominant frequencies of these

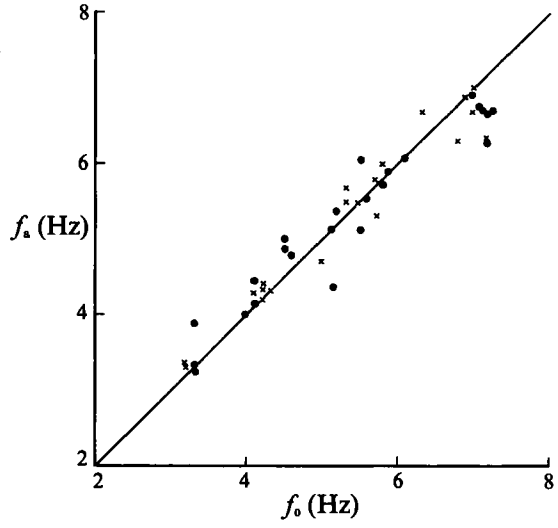

FIGURE 15. Wind wave frequencies before (f_0) and after (f_s) suppression by long-wave groups. The crosses are spectral peak frequencies and the solid points are derived from counting wave crests.

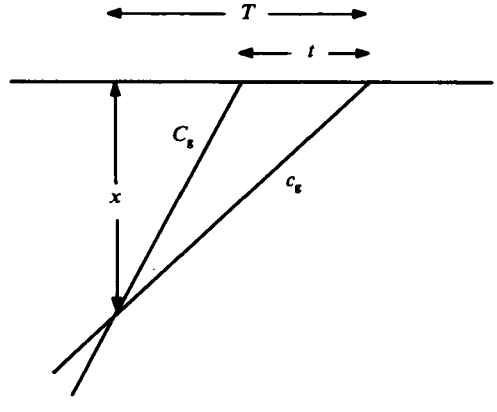

FIGURE 16. The effective duration T of wind-wave growth following the groups which move with group velocity C_g, in terms of the time interval t measured at a fixed point.

suppressed waves were however not significantly different from what they had been initially, though their amplitudes were reduced. Figure 15 plots frequencies before and after suppression measured in two different ways – by counting the number of wave crests per unit time in a number of individual realizations of each experiment and from the peak frequencies of spectra measured in 5 s time intervals before and just after the group. Though the numerical values of the frequencies found in these two ways differ somewhat, no systematic frequency shift is evident. The dominant waves remaining after the passage of the group are then substantially below their equilibrium energy levels and they then begin to recovery under the continued action of the wind.

The rate at which this occurs allows us to estimate their growth rate in a context in which the influence of wave–wave interactions is reduced, but in which allowance must be made for the moving fetch. Suppose, as illustrated in figure 16, short waves emerge from the rear of the long-wave group some distance x upwind of an

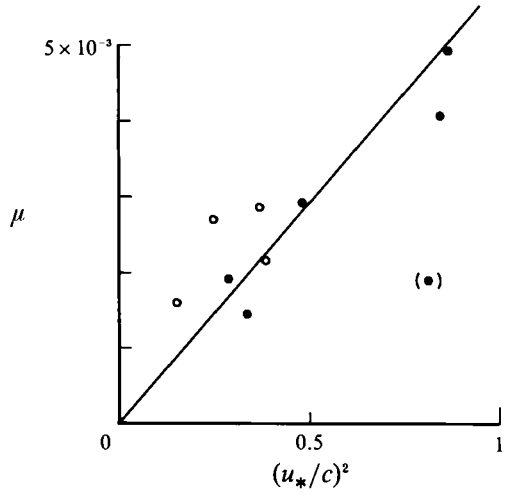

FIGURE 17. The coupling coefficient for wave regeneration by wind, following suppression. The open circles are for $u_* = 15$ cm s^{-1}; solid circles for $u_* = 27$ cm s^{-1}.

observation point; their energy will arrive at the observation point a time T later, where $x = c_g T$. At the observation point, however, they arrive a shorter time t after the rear of the group has passed *this* point, the long-wave group having propagated the distance x to this point in the time $(T-t)$, moving with its group velocity C_g. Thus

$$x = c_g T = C_g(T-t),$$

so that the duraction of wind input during the recovery is greater than the elapsed time measured at the observation point:

$$T = \frac{C_g}{C_g - c_g} t = \frac{\sigma}{\sigma - n} t, \tag{5.1}$$

where σ and n are the short- and long-wave frequencies respectively. If the coupling coefficient between wind and waves is represented by μ, then

$$\overline{\zeta^2} \propto \exp(\mu\sigma T) = \exp \gamma t,$$

where the growth rate observed at the fixed observation point

$$\gamma = \mu\sigma^2/(\sigma - n).$$

Accordingly, the coupling coefficient is

$$\mu = \gamma(\sigma - n)/\sigma^2. \tag{5.2}$$

Experiments were selected in which the energy suppression by the long waves was 50% or more (a rather small fraction of the total number as can be seen from figure 14), and γ-values were found by fitting an expression of the form $\overline{\zeta^2} = A \exp \gamma t$ to the ensemble-averaged measurements beginning at the minimum of $\overline{\zeta^2}$ and ending before the abrupt rise. The coupling coefficients were calculated from (5.2) and the results are plotted in figure 17 as a function of $(u_*/c)^2$ where u_* is the appropriate *mean* friction velocity. Except for one stray point, the results are reasonably consistent with a straight line fit $\mu = 5.2 \times 10^{-3} (u_*/c)^2$, of the form suggested by Plant (1982) to be appropriate when $(c/u_*) < 10$. The numerical coefficient is however con-

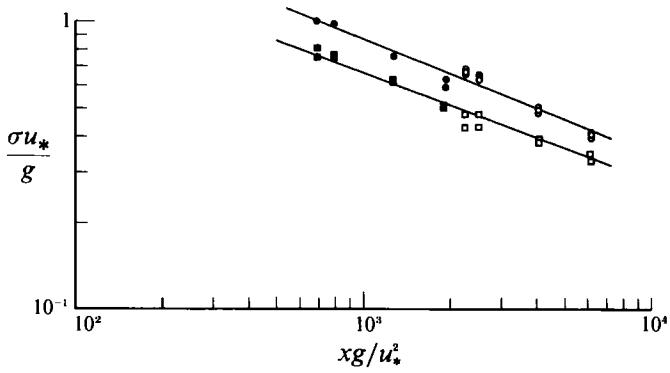

FIGURE 18. The variation of dimensionless frequency with fetch in the undisturbed wind field (circles) and in the wave energy front (squares). Open symboles are for $u_* = 15$ cm s^{-1}, solid ones $u_* = 27$ cm s^{-1}.

siderably smaller than the value found by Plant (0.04) in his examination of measurements of wave growth in uniform wind fields. In the present experiments, the wind incident upon the smooth regeneration region has just passed over the much rougher surface behind the wave energy front, so that the actual local surface stress and friction velocity on this newly smooth surface is certainly considerably less than on the rough surface upwind and less than the *average* value measured in the experiment. Although there seemed no way to measure the local stress directly, the use of too high a value of u_* in expression (5.2) for μ would reduce the numerical coefficient substantially. Another possibility, suggested by a referee, is that the turbulence in the water produced by wave breaking inhibits the growth of the local wind sea. In either event, the experimental results do indicate that the wind-wave field regenerates more slowly after suppression by a long-wave group than one would expect from Plant's formula, using an averaged value of u_*.

6. The wave energy front

6.1. *Wave characteristics*

As described earlier, the gradual recovery of the short waves under the influence of the wind is terminated by the abrupt arrival of the wave energy front in which $\overline{\zeta^2}$ is larger and the dominant frequency smaller than in the initial undisturbed field. Figure 9 already shows that the dominant frequency just behind the front decreases with increasing fetch, and figure 18 indicates that the variations in spectral peak frequency with fetch can be expressed in terms of the same dimensionless variables as customarily used for a statistically steady wave field. The physics involved is however almost certainly very different. In a statistically steady wave field, the decrease of dominant frequency with fetch is largely the result of nonlinear wave–wave interactions in Fourier space and the movement towards lower frequencies of the steep forward face of the spectrum. In this experiment, the steep forward face of the energy density is in physical space as the waves propagate into the region where the local wind sea has been suppressed. Linear dispersion allows the lower frequencies to propagate faster as they are amplified by the wind, leaving higher frequencies behind; this is consistent with the relative narrowness of the local spectra in this region mentioned earlier. The propagation speed of the energy front is significantly greater than would be expected from the group velocity corresponding

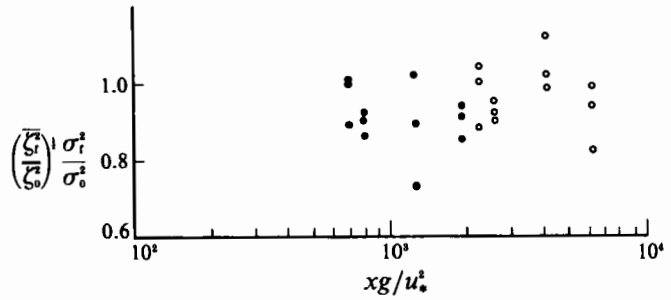

FIGURE 19. 'Significant slopes' in the wave energy front relative to values in the undisturbed wind-wave field. Open and solid symbols as in figure 10.

u_*	15 cm s^{-1}					27 cm s^{-1}		
$(\alpha k)_m$ in group	0.16	0.16	0.23	0.28	0.28	0.17	0.28	0.28
Fetch interval	A	B	A	A	B	A	A	B
$C_t = \Delta X/\Delta T$ (cm s^{-1})	26.5	29.5	26.2	28.0	30.0	33.0	32.5	35.0
$\overline{c_g}$ (cm s^{-1})	19.7	22.2	19.1	20.5	22.7	21.9	21.6	24.9
δc (cm s^{-1})	6.8	7.3	7.1	7.5	7.3	11.1	10.9	10.1
$\delta c/u_*$	0.45	0.48	0.47	0.50	0.48	0.41	0.40	0.38

TABLE 2. Measured propagation of wave energy fronts. Fetch interval A is from 5.9 to 9.5 m ($\Delta X = 3.6$ m) and B from 9.5 to 14.4 m. The average group velocity $\overline{c_g}$ is calculated from the mean peak frequency just behind the energy front and the residual δc is the difference between C_t and $\overline{c_g}$.

to the local frequency as table 2 indicates. Part of this increased speed is probably associated with the continued leakage by dispersion of lower-frequency components ahead of the front and their subsequent amplification by the wind. Part is also likely to be the result of induced circulation in the tank – it is easy to show that in a uniform current U, waves with an apparent frequency n have an energy flux velocity of $\frac{3}{2}U + (g/2n)$ when $nU/g \ll 1$. It was noted in §2 that the propagation speed of the long-wave groups was 2–3 cm s^{-1} faster than would be expected in still water, suggesting the presence of some wind-induced circulation. In the wave energy front, the dominant wavelength is of order one tenth of that in the mechanically generated group, so that one might anticipate a greater advective contribution from such a circulation, approximately proportional to u_* as table 2 might suggest.

Values of the significant slope $(\overline{\zeta^2})^{\frac{1}{2}}\sigma^2/g$ were found just behind the front and compared with those in the undisturbed field at the same fetch and wind speed. As before, $\overline{\zeta^2}$ was found by integration of local spectra with low frequencies removed and σ was taken as the frequency of the spectral peak. From figure 19, there seems to be no systematic dependence of the significant slope ratio upon fetch nor any significant difference in the ratio from unity, the mean and standard deviation being 0.94 and 0.08 respectively. Apparently, the significant slopes attained by these waves under equilibrium or saturation conditions at a given u_* are virtually independent of the conditions under which this condition is attained, whether initially, in the breaking waves in the leading portion of the group, or behind the wave energy front.

6.2. *Is the front an artefact of this experiment?*

The present set of experiments provides little insight into the genesis of the wave energy front, though it is apparent from figure 1 that it arises near the upwind end of the tank following the generation of the long-wave group. The onset and cessation of the paddle motion do create local disturbances in addition to the radiated wave pulse, which may have seeded the phenomenon. There was sometimes some breaking of these waves close to the paddle, but because of the rapidity and randomness of the processes, it was difficult to discern by eye whether these disturbances evolved into the front further down the tank. A subsequent series of experiments, which will be described in due course, was designed to damp out these (uncontrolled) disturbances and then to replace them by a controlled perturbation, which again led to the appearance of the energy front. There are, of course, profound dynamical differences between ordinary fetch-limited growth and the fetch-limited growth of waves on a water surface on which small-scale waves have been suppressed by the prior passage of the wave group. Waves just behind the front are growing under the action of the wind in the absence of the shorter components that are present in a steady fetch-limited situation (or a homogeneous, duration-limited one) since these, at higher frequencies, are left behind. Sideband instabilities may develop in time or equivalently with distance behind the front but there is less opportunity for resonant wave–wave interactions to transfer energy from the dominant frequencies near the front than there is in the usual fetch-limited case.

One might anticipate that the phenomenon is likely to occur also in extra-laboratory situations. A moving ship generates a Kelvin wave group and sometimes solitary wave packets (Brown *et al.* 1989) that radiate outwards (as in our experiments), suppressing shorter, background wind-generated waves. The turbulent boundary layer around the ship and the turbulent wake behind it are replete with disturbances that can trigger a wave energy front which can be expected to develop, moving outwards more slowly than the longer wave groups, until it merges into the regenerated wave field ahead of it. It is tempting to conjecture that this may be associated with the narrow 'V-wakes' (Munk, Scully-Power & Zachariasen 1987) sometimes observed at angles of 2° or 3° both optically and by synthetic aperture radar. Only further work and time will tell.

It is a pleasure to acknowledge the support of the Office of Naval Research under grant N00014-90-J-1482 (for O.M.P.) and grant N00014-90-J-1450 (for J.S.C.).

REFERENCES

Banner, W. J. & Melville, W. K. 1976 On the separation of air flow over water waves. *J. Fluid Mech.* **77**, 825–842.

Brown, E. D., Buchsbaum, S. B., Hall, R. E., Penhume, J. P., Schmitt, K. F., Watson, K. M. & Wyatt, D. C. 1989 Observations of a solitary wave packet in the Kelvin wake of a ship. *J. Fluid Mech.* **240**, 309–337.

Donelan, M. A. 1987 The effect of swell on the growth of wind waves. *Technical Digest* vol. 8, pp.18–23. Johns Hopkins APL.

Huang, N. E. & Long, S. R. 1980 An experimetal study of the surface elevation probability distribution and statistics of wind-generated waves. *J. Fluid Mech.* **101**, 179–200.

Mitsuyasu, H. 1966 Interaction between water waves and wind (I). *Rep. Res. Inst. Appl. Mech., Kyushu Univ.* **14**, 57–88.

Mitsuyasu, H. 1968 On the growth of the spectrum of wind-generated waves, I. *Rep. Res. Inst. Appl. Mech., Kyushu Univ.* **14**, 459–482.

MUNK, W. H., SCULLY-POWER, P. & ZACHARIASEN, F. 1987 Ships from space. *Proc. R. Soc. Lond.* A, **412**, 231–254.

PHILIPS, O. M. 1981 The dispersion of short wavelets in the presence of a dominant long wave. *J. Fluid Mech.* **107**, 465–485.

PHILLIPS, O. M. & BANNER, M. L. 1974 Wave breaking in the presence of wind drift and swell. *J. Fluid Mech.* **66**, 625–640.

PLANT, W. J. 1982 A relationship between wind stress and wave slope. *J. Geophys. Res.* **87**, 1961–1967.

WHITHAM, G. B. 1974 *Linear and Nonlinear Waves.* Wiley-Interscience. 636 pp.